

## EnVision: taking the pulse of our twin planet

**Richard C. Ghail · Colin Wilson · Marina Galand · David Hall · Chris Cochrane · Philippa Mason · Joern Helbert · Franck MontMessin · Sanjay Limaye · Manish Patel · Neil Bowles · Daphne Stam · Jan-Erik Wahlgren · Fabio Rocca · David Waltham · Tamsin A. Mather · Juliet Biggs · Matthew Genge · Philippe Paillou · Karl Mitchell · Lionel Wilson · Upendra N. Singh**

Received: 30 March 2011 / Accepted: 19 July 2011  
© Springer Science+Business Media B.V. 2011

**Abstract** EnVision is an ambitious but low-risk response to ESA's call for a medium-size mission opportunity for a launch in 2022. Venus is the planet most similar to Earth in mass, bulk properties and orbital distance, but has evolved to become extremely hostile to life. EnVision's 5-year mission objectives are

---

R. C. Ghail (✉) · M. Galand · C. Cochrane · P. Mason · M. Genge  
Imperial College London, London SW7 2AZ, UK  
e-mail: r.ghail@imperial.ac.uk

C. Wilson · N. Bowles  
University of Oxford, Oxford OX1 3PU, UK

D. Hall  
Astrium, Portsmouth, PO3 5PU, UK

J. Helbert  
DLR, 12489 Berlin, Deutschland

F. MontMessin  
LATMOS, 75252 Paris, France

S. Limaye  
University of Wisconsin-Madison, Madison 53706, USA

M. Patel  
Open University, Milton Keynes, MK7 6AA, UK

D. Stam  
SRON Netherlands Institute for Space Research, Utrecht, Netherlands

J. -E. Wahlgren  
Swedish Institute of Space Physics, Uppsala University, 75105 Uppsala, Sweden

to determine the nature of and rate of change caused by geological and atmospheric processes, to distinguish between competing theories about its evolution and to help predict the habitability of extrasolar planets. Three instrument suites will address specific surface, atmosphere and ionosphere science goals. The Surface Science Suite consists of a 2.2 m<sup>2</sup> radar antenna with Interferometer, Radiometer and Altimeter operating modes, supported by a complementary IR surface emissivity mapper and an advanced accelerometer for orbit control and gravity mapping. This suite will determine topographic changes caused by volcanic, tectonic and atmospheric processes at rates as low as 1 mm a<sup>-1</sup>. The Atmosphere Science Suite consists of a Doppler LIDAR for cloud top altitude, wind speed and mesospheric structure mapping, complemented by IR and UV spectrometers and a spectrophotopolarimeter, all designed to map the dynamic features and compositions of the clouds and middle atmosphere to identify the effects of volcanic and solar processes. The Ionosphere Science Suite uses a double Langmuir probe and vector magnetometer to understand the behaviour and long-term evolution of the ionosphere and induced magnetosphere. The suite also includes an interplanetary particle analyser to determine the delivery rate of water and other components to the atmosphere.

**Keywords** Venus tectonics · Venus atmosphere · Venus ionosphere · InSAR · LIDAR

---

F. Rocca  
Politecnico di Milano, 20133 Milan, Italy

D. Waltham  
Royal Holloway, University of London, Egham, TW20 0EX, UK

T. A. Mather  
University of Oxford, Oxford OX1 3AN, UK

J. Biggs  
University of Bristol, Bristol, BS8 1RJ, UK

P. Paillou  
University of Bordeaux, 33270 Floirac, France

K. Mitchell  
Jet Propulsion Laboratory, California Institute of Technology, Pasadena, CA 91109, USA

L. Wilson  
Lancaster University, Lancaster, LA1 4YQ, UK

U. N. Singh  
NASA Langley Research Center, Hampton, VA 23681-2199, USA

## 1 Science case

### 1.1 Surface science

The major unknown in Venus science is its rate and style of geological activity and the influence any activity has on its atmosphere. There is some evidence for recent geological activity [1, 26], particularly from Venus Express data [44] but as yet no accepted model that can explain the observed range of geological features, the near-random distribution of craters, and the inferred global heat production.

Three possible geodynamic frameworks have been proposed, each with profound implications for understanding the nature and habitability of terrestrial planets in other stellar systems. The episodic resurfacing model [5, 6, 50–52] proposes a short-lived but intense period of activity  $\sim 750$  Ma ago, followed by a long period of quiescence that is consistent with the impact crater distribution. This model gained early wide acceptance but its prediction of almost no volcanic and tectonic activity at the present day seem inconsistent with geological observations. These observations led to proposals involving some form of plate-like movement (e.g., [20, 21, 31, 36, 43, 49]) that imply ongoing volcanic and tectonic activity similar to terrestrial continental interiors. Quantitative estimates are difficult to determine but perhaps  $5\text{--}10$  mm  $\text{a}^{-1}$  local tectonic movement and more than  $\sim 0.5$  km $^3$   $\text{a}^{-1}$  in global extrusive activity [47] are reasonable. However, these proposals have difficulty explaining the globally near-random distribution of impact craters and rely on specific local relationships. These two end-member models are not mutually exclusive and many authors therefore favour an intermediate level of dominantly plume-related volcanic activity (e.g., [10, 23, 26, 40]) and localised tectonic activity.

Distinguishing between these end member models and intermediate models of current surface activity requires very precise measurements of the long term rates of surface change. The aim of the surface science suite is to characterise the nature and rate of geological change on Venus by clarifying shallow and deep structures within the crust and upper mantle; identifying seismic events (earthquakes) and quantifying mean strain rates; detecting active magma chambers and monitoring long-term volcanic processes; and characterising areas of aeolian activity and mass wasting.

The extreme surface conditions on Venus require that these science goals must be addressed by orbital remote sensing, including interferometric synthetic aperture radar (InSAR) data, gravity data, altimetric data and multispectral infrared data. Deep structures can be inferred from long-wavelength topographic and gravity/geoid data. Shallow structures, such as magma chambers, can be inferred from short-wavelength gravity anomalies and, if active, from regional changes in elevation identified from interferometric synthetic aperture radar (InSAR) data. Volcanic activity causes changes in surface elevation detectable by InSAR and changes in infrared emissivity properties; active eruptions will be directly detectable in infrared data. Aeolian activity and mass wasting will cause decoherence of the InSAR data between orbit

cycles, as well as possible changes in infrared emissivity. These data are now routinely acquired from Earth orbit for the terrestrial environment but have never before been attempted at another planet at the precision required to achieve meaningful results and in the absence of a global positioning system or ground control network.

Advances in technology, data acquisition and processing, and satellite control and tracking, mean that it is now feasible to do so. Furthermore, the proximity of Venus to Earth, the relatively calm (if extreme) surface conditions and lack of water, the absence of a large satellite and its moderately well-known geoid (to about  $2^\circ$ ) and topography (to better than  $1^\circ$ ) all help to ease the technical demands on the mission.

The primary observational objective is to map the radar phase returned by the InSAR system, from which will be derived maps of surface displacement and loss of coherence. Ancillary data collected to achieve this objective include high-resolution gravity data and the radar backscatter intensity, atmospheric transmissivity, surface elevation, emissivity and reflectivity, and will in themselves provide an order of magnitude improvement over Magellan data.

An assessment of the rate and distribution of surface displacement and loss of coherence will distinguish between the end-member and intermediate models of surface displacement. The episodic resurfacing model predicts that no surface displacement should be detected; the plate model predicts that surface displacements should be concentrated along plate boundary zones with minimal displacements in plate interiors; while the intermediate models predict that surface displacements should be associated with volcano-tectonic centres distributed essentially at random. While loss of coherence over large areas might make it more difficult to distinguish between these models, it would itself imply much greater levels of aeolian activity than expected on the basis of Magellan observations and would therefore be a profoundly interesting result in itself.

On Earth, InSAR measurements of surface displacements have provided a versatile means to evaluate spatial and temporal scales of magma storage within a range of tectonic settings, including rift zones (e.g., [7]), continental settings [12, 54], and subduction zones [18]. Changing pressures within crustal magma reservoirs caused by, amongst other things, magma and/or volatile fluxes produce changes in volcano shape on the scale of centimetres to metres (e.g., [55]). Deformation of volcanic products post emplacement, such as slow downslope creep of volcanic edifices (e.g., [14]) and the thermal contraction of cooling lava flows (e.g., [46]) have also been successfully detected. InSAR data from Venus would provide the first observations of the processes of magmatic activity on another planet, including both magma storage and effusion. The observed number of magmatically active centres, their spatial distribution (either random or associated with possible plate boundaries) and rates of deformation are all key to distinguishing between the competing geodynamic frameworks discussed earlier.

Of equal importance is the detection of seismic events and aseismic creep that are characteristic of tectonic deformation. Each geodynamic framework

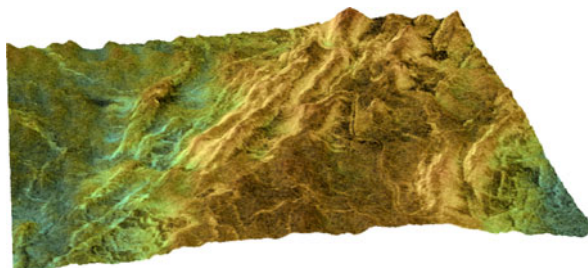


**Fig. 1** Magellan Stereo-SAR view of a Canali in Lemketchen Dorsa. Offsets (dog-legs) along the course of the canali indicate a long period of contemporaneous canali and ridge activity. Accumulations of loose sediment (dark areas *top right*) are also apparent between some of the ridges

predicts a different frequency and distribution of seismicity and different rates of aseismic deformation. Observations of these processes will therefore distinguish between competing framework models; a null result (from coherent returns) would be consistent with catastrophic global resurfacing, while linear zones of seismicity would be consistent with active subcrustal plate tectonics.

Although Venus is apparently largely devoid of sediments, landers have shown that the surface is strongly weathered and may consist of sedimentary rocks [16]; dunes, wind-streaks and landslides have all been detected in Magellan data. Particularly enigmatic are the canali (Fig. 1): moderately sinuous, parallel-sided channels crossing the plains, with widths of a few km and lengths of hundreds to thousands of km [2, 28] that may represent exotic lava flow channels [29], ancient river beds [27] or the result of turbidity currents [53] in the dense atmosphere. If any or all of these features are active, such activity will cause a loss of coherence between successive images; tracking that loss will indicate how active the Venus surface environment is. The EnVision antenna can send and receive both horizontally (H) and vertically (V) polarised waves. The H and V polarisation responses of sediments (and impact ejecta) is very different to that of bare rock [11], enabling EnVision to quickly map the distribution of sediments and bare rock; such information will reveal both the nature of surface environmental processes on Venus and the location of fresh (and by implication, young) surface rocks.

The maturity of these studies on Earth is such that data returned from Venus can confidently be understood within a solid theoretical framework developed from coupled terrestrial InSAR data and ground-truth observations (e.g., [18]), given the absence of ground-truth data on Venus.

## 1.2 Cloud and atmosphere science

Long-term changes in the atmosphere may be caused by external processes (flares, solar cycles, changes in obliquity, atmospheric erosion by the solar wind or accretion of interplanetary dust, etc.), or by surface interactions (volcanic

emissions, surface weathering, tectonic cycles, etc.). The clouds are likely to be particularly sensitive to these processes [9, 48].

The low circular orbit of Envision and the relatively high primary power and return data rate required for InSAR operations make the spacecraft an ideal platform for a complementary LIDAR instrument. This instrument will serve two main science goals: direct measurement of mesospheric winds, and study of cloud-top properties. Direct measurement of mesospheric winds from a Doppler LIDAR represents a huge improvement on these indirect techniques and will finally permit the measurement of mean circulation and wind transients associated with dynamics at all latitudes, including the complex polar vortex region. The cloud-top vertical backscatter coefficient profiles provided by the LIDAR will permit the study of the many morphological phenomena revealed by the Venus Monitoring Camera (VMC) on Venus Express.

The Thermal Infrared Mesospheric Mapping Spectrometer (TIMMS), operating in the 5 to 25  $\mu\text{m}$  wavelength range, will measure temperature profiles from 65 to 90 km altitude on the dayside, providing context for the LIDAR's direct wind measurements. It will also measure abundances of stratospheric constituents including CO, H<sub>2</sub>O and SO<sub>2</sub> and cloud-top temperatures.

Complementing TIMMS will be a UV Spectrometer Channel (UVSC), which will map the temporal and spatial variability in the distribution of SO<sub>2</sub>, potentially revealing discrete volcanic emissions [15] and the impact of solar effects and other external processes [35].

The LIDAR's measurement of cloud-top structure returns vertical profiles of the backscatter coefficient; to convert this into more meaningful quantities such as cloud particle number density requires further information about the cloud particles. This can be obtained by measuring polarisation and intensity phase functions. The Spectrophotopolarimeter for Planetary EXploration (SPEX) will determine the polarisation state as well as the intensity of light in the 400 to 800 nm range in order to reveal the microphysical properties of the cloud layers measured by the LIDAR.

### 1.3 Ionosphere science

The upper atmosphere of Venus is partially ionised by the action of solar EUV, X-ray and  $\gamma$ -ray radiation, energetic impacting electrons and ions from the surrounding space environment as well as cosmic radiation. The resulting ionosphere is electrically conducting and couples electro-dynamically to the external magnetised plasma flow (the solar wind) that Venus is exposed to. In the case of unmagnetised bodies with a well-developed ionosphere like Venus, this interaction leads to the formation of an induced magnetosphere enveloping the planetary body, which mediates the escape of the ionospheric plasma to the surrounding space and contributes to the atmospheric erosion of these bodies. Atmospheric erosion, along with atmospheric refilling, is of key importance for the climate evolution of Venus over geological timescales (e.g., [48]).

While photochemical equilibrium prevails in the deep ionosphere, the upper ionospheric layers are strongly affected by transport and atmospheric loss mechanisms (e.g., [19]). However, the type of loss varies with regions above or below the ionopause. This boundary, defined as the location where thermal ionospheric plasma pressure balances magnetic pressure from the magnetosheath, is highly variable depending on physical parameters such as solar wind dynamic pressure and solar activity [41]. It increases with solar zenith angle, being as low as 200 km in extreme cases, and reaching altitudes of 1000 km at the solar terminator. Below the ionopause, day-to-night transport is the main source of the nightside ionosphere. While most of the nightward ions flow towards the nightside, some escape through the filamentary, stretched magnetised tail. Ions escaping through the plasma sheet at the centre of the plasma wake are primarily H<sup>+</sup>, O<sup>+</sup>, and He<sup>+</sup> [3]. Atmospheric total escape rates of O<sup>+</sup> ions have been estimated to be  $10^{24}$  to  $10^{26}$  s<sup>-1</sup> (e.g., [4, 32]). Atmospheric loss through ion pick-up occurs above the ionopause, as shown through the analysis of PVO plasma dataset with rate of the order of  $\sim 5 \times 10^{24}$  ions s<sup>-1</sup> [38]. Such a loss mechanism is strongly enhanced, by up to two orders of magnitude, during solar activity and during coronal mass ejections [34].

At an altitude of 300 km, EnVision will be examining the topside ionospheric region in-situ. Through measurements with a double Langmuir probe and vector magnetometer, it will be possible to assess the variability of the ionopause on the dayside, especially during periods of strong solar wind dynamic pressure and/or low solar activity. For part of the sunlit orbit below the ionopause, electron density profiles of the eroded ionosphere will be measured by the Langmuir probe. The magnetometer observations are expected to constrain the filamentary, induced tail from which ionospheric outflows are escaping. Unlike previous probes that had elliptical orbits, the 300 km constant altitude of EnVision offers the first ionospheric observations from a circular orbit. It is the perfect opportunity to study the temporal variability of the region and to compare ionospheric and magnetic characteristics in regions symmetric around noon, such as the dawn/dusk regions.

## 2 Instruments

The EnVision mission will address its science goals with three groups of complementary instruments: the Surface Science Suite, the Atmosphere Science Suite, and the Ionosphere Science Suite. The instruments in each suite are listed in Tables 1 and 2 below, together with baseline estimates of their TRL, mass and power requirements.

### 2.1 EnVision antenna

The antenna for the EnVision Radar will use panels from the antenna subsystem (SAS) of the Sentinel-1 mission (which is part of the ESA GMES constellation). Each antenna panel (Fig. 2) comprises a column of 20 H and V

**Table 1** Instruments in each science suite

		TRL	Mass/kg	Power/W
Surface science suite				
EnVision antenna and radar central electronics		7	190.1	
Interferometer mode 1	EAIM-1			545.0
Radiometer altimeter mode	EARAM			350.0
Venus emissivity mapper	VEM	5	5.4	18.5
Venus advanced accelerometer	VAA	8	3.0	3.0
Atmosphere science suite				
EnVision doppler LIDAR	D-LDR	4	25.0	70.0
Spectrophotopolarimeter	SPEX	6	2.0	5.0
Thermal infrared mesospheric mapping spectrometer	TIMMS	5	3.0	2.0
UV spectrometer channel	UVSC	5	0.5	1.0
Ionosphere science suite				
EnVision double Langmuir probe	ELP	8	1.0	2.3
Venus vector magnetometer	VVM	7	1.0	1.0
Venus interplanetary particle analyser	VIPA	8	4.2	2.4

polarised pairs of slotted waveguide sub-arrays. The complete EnVision radar antenna consists of three of these panels and measures 2.634 m (azimuth) by 0.84 m (elevation), giving a total area of 2.2 m<sup>2</sup>. It appears as a 3 (azimuth) by 20 (elevation) array of radiator pairs in which each waveguide is excited by a dedicated transmit receive module (TRM). 60 TRMs excite the H polar waveguides and another 60 TRMs excite the V polar waveguides. Only one polarisation is excited at any instant. The peak RF power from each TRM is 15 W, providing a peak RF power to the antenna of 900 W. The mechanical boresight of the antenna is set at 13.0° away from nadir.

### 2.1.1 Interferometer mode

The primary role of the SAR system is to acquire repeated interferometric synthetic aperture radar (InSAR) data from at least three of eight or more orbit cycles, each cycle taking one sidereal Venus day (243 Earth days) during which the entire surface of the planet rotates beneath the orbit. Data from the first two orbit cycles are required to produce an interferometric digital elevation model; data from at least one more cycle (separated in time by several orbit cycles) are combined with data from the first two cycles to detect interferometric (subwavelength) changes in ground elevation during the intervening period. Rates of change in surface elevation as low as 1 mm a<sup>-1</sup> can be detected over the 5-year design lifespan of EnVision; an extended mission duration would permit the detection of even lower rates of change. The nominal mission proposes the use of Cycles 5 and 8 for repeat interferometry, providing two opportunities for change detection. The remaining orbit cycles (i.e., Cycles 3, 4, 6 and 7) will be used to collect supplementary data, such as the HV, VH and VV response of ground targets, alternative imaging geometries, additional radiometer and altimeter data.

**Table 2** EnVision instrument science objectives

	Science objective	Measurement objective	Measured parameters	Precision/accuracy
Surface science suite E AIM-1	Quantify the current rate of geological activity on Venus.	Determine the rate of change of the ground surface elevation.	Interferometric fringes and loss of coherence between image pairs.	30 m spatial resolution; Phase: 1/32 wavelength, or >0.7 mm vertical displacement.
EARAM	Map global geomorphology, stratigraphy and weathering processes.	High-resolution global topographic, radiometric and transmissivity data.	Nadir pulse return time and power; interleaved passive emitted power.	Altimeter: $\pm 1$ m vertical. Radiometer: $\pm 0.75$ K $3.6 \times 0.6$ km spatial at 10.1 km track spacing.
VEM	Identification of anomalous terrain, e.g., granite, fresh flows, plus cloud processes.	Surface mineralogy; near surface water vapour; cloud microphysics and thickness.	13 near infrared spectral bands between 0.8 and 1.8 $\mu$ m.	Sensitivity 3 $\times$ better than VIRTIS on Venus Express. 20 nm bandwidth.
VAA	Discriminate 100 km-scale subsurface structures at individual geomorphic features.	360 degree and order spherical harmonic gravity field and geoid.	Voltage required to resist acceleration of a controlled mass by gravitational field.	Gravity: $\pm 5 \times 10^{-5}$ m s $^{-2}$ ; Geoid: $\pm 0.5$ m; 53 km spatial resolution.
Atmosphere science suite D-LDR	Structure and dynamics of the mesosphere and uppermost cloud properties.	Mesospheric wind velocity and cloud particle density structure.	Vertical profile of the backscatter coefficient and the doppler shift of transmitted laser pulse.	Windspeed better than 20 m s $^{-1}$ ; < 1 km vertical resolution; $\sim 50$ km spatial resolution.
SPEX	Cloud particle microphysics, (size, shape, composition).	Polarisation state and intensity of light between 400 and 750 nm.	Scattered intensity I, degree and direction of polarisation P and $\chi$ .	Resolution: 2 nm flux; 20 nm and 0.005 polarisation.
TMMS	Temperature profile 65 to 90 km; CO, H <sub>2</sub> O and SO <sub>2</sub> abundances.	Fourier-transformed spatially-resolved interferogram spectra.	Spectra between 6 and 25 $\mu$ m, spatially resolved.	Resolution: 5 cm $^{-1}$ spectral, 15 km spatial.
UVSC	Cloud top SO <sub>2</sub> concentration and the spatial distribution of the unknown UV absorber.	Ultraviolet spectra.	Spectra between 180 to 360 nm.	Resolution: <2 nm spectral; 5 km spatial.

Science objective	Measurement objective	Measured parameters	Precision/accuracy
Ionosphere science suite			
ELP	Map the structure and dynamics of the ionosphere and identify ionisation sources.	Plasma electron temperature, potential and density.	Density: $<10^{12} \text{ m}^{-3}$ ; electron energy: $10^{-21} - 10^{-18} \text{ J}$ ; Potential: $\pm 20 \text{ V}$ , $<1 \text{ Hz}$ .
VVM	Map the structure and dynamics of the induced magnetosphere.	Vector and intensity of the magnetic field.	50 vectors $\text{s}^{-1}$ , $\pm 1 \text{ nT}$ , $<4 \text{ Hz}$ .
VIPA	Mass and types of interplanetary dust (especially water) at Venus.	Interplanetary dust particle mass and energy.	Impact-induced plasma charge and energy. 1.2 $\times 10^{-13}$ at 5 $\text{km s}^{-1}$ ; 2.0 $\times 10^{-15}$ at 20 $\text{km s}^{-1}$ .

**Table 2** (continued)

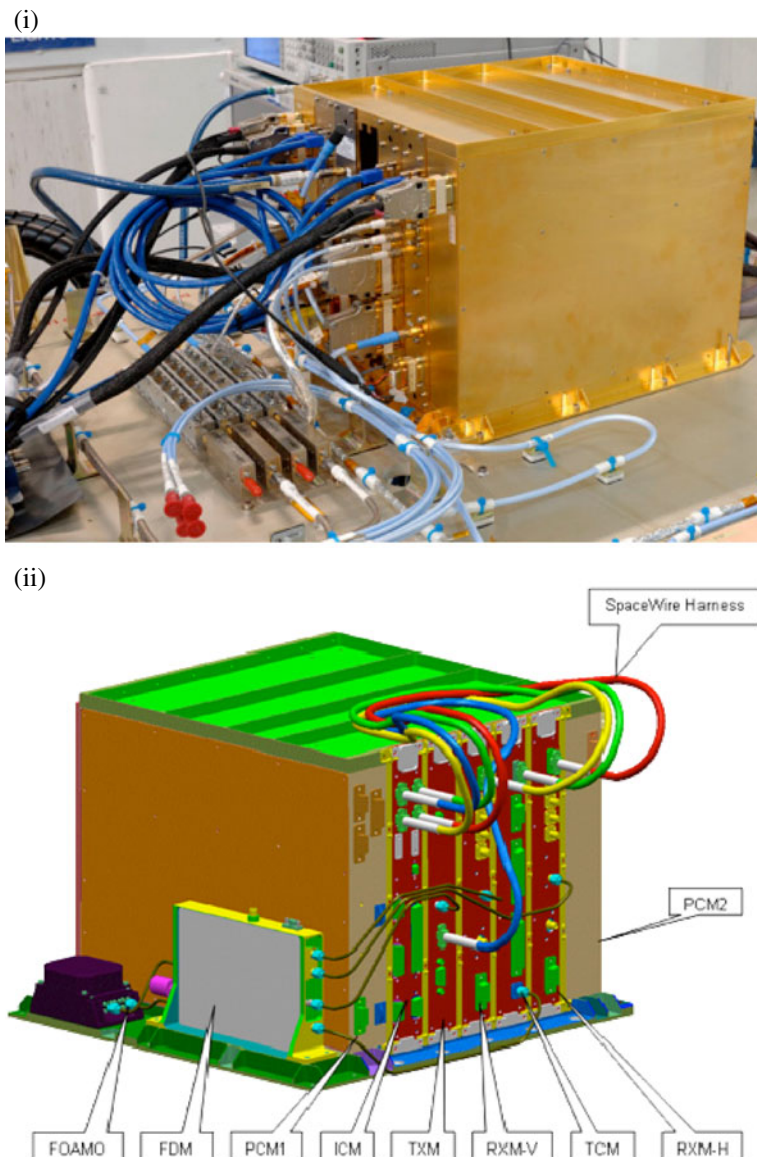


**Fig. 2** Radar central electronics subsystem. *i* photograph of the RCE assembly (only one of two identical RCEs is shown). *ii* RCE mechanical block diagram

The principal constraints on the EAIM are orbit control and data volume. Accurate knowledge of the position of the sensor in its orbit and the ability to return the sensor to the same orbital position (to within  $\sim 100$  m) in the next cycle are vital for successful interferometry; a mission requirement is therefore

that the orbital position errors do not exceed 100 m. The low circular orbit of EnVision and the near spherical shape of Venus reduce the complexity of the orbital determination but meeting this requirement necessarily entails an improved determination of the Venus geoid, achieved in part by the Venus Advanced Accelerometer experiment. The spacecraft must also be precisely oriented in space, with the antenna pointing in the correct direction to within a fraction of a beam width. This requirement is relatively routine and EnVision's stable bus and Orbital Star Trackers are designed for that purpose.

The EAIM will operate in two modes: in Mode 1, the normal state, the radar will operate for 9 min per orbit, acquiring an image swath 26.1 km wide and up to 3680 km long, at a resolution of 60 m along- and across-track; the optional high-resolution Mode 2 the radar will operate for about 5 min and acquire a 26.1 km wide image swath up to 2045 km long, at a resolution of 30 m along- and across-track.

The three-panel antenna size results from spacecraft mass and power constraints; maintenance of adequate performance requires that it operate from a lower (300 km) orbit than is usual for terrestrial SARs such as Sentinel-1. A two-panel option was considered but rejected on the basis of an unacceptable reduction in sensitivity from  $-16.5$  to  $-10.7$  dB, which could not be improved by further lowering of the orbit because of the high atmospheric drag at lower altitudes.

With the three-panel option, several modes are possible. Figure 3 illustrates the swath selection procedure. For horizontally-polarised transmit and receive (HH) and a boresight of  $13^\circ$ , the optimal swath selected is IS3. IS2 is an approximation to the altimeter mode (EAAM). IS1, IS4 and IS5 are all acceptable modes but have either higher ambiguities or lower sensitivity. For the purposes of this study, IS3 is used for both EAIM-1 (60 m resolution) and EAIM-2 (30 m resolution) but further optimisation of the system is possible. The IS3 parameters are listed in Table 3 below, for modes EAIM-1 and EAIM-2.

The full data rates quoted are based on 4-bit I, 4-bit Q adaptive quantisation with the RCE processor operating in HH mode. The rate is slightly more than double this when both HH and VV data are required. Assuming that only HH polarisation is required and applying a 3-bit I, 3-bit Q adaptive quantisation, a complete pole-to-pole image swath at 30-m resolution (EAIM-2) would take slightly more than 45 min and require the transmission of 14.822 GB of data to Earth. This requirement is reduced because operation of the radar system is restricted thermally to about 15 to 20 min per orbit, since a dedicated cooling system cannot be provided within the mass, power and budget constraints of an M-class mission. Even so, in EAIM-2 mode, 4.781 GB of data are generated in a 15 min period. Lowering the resolution to 60 m (EAIM-1) only reduces the acquired data volume to 2.725 GB.

Power constraints mean that these data volumes must normally be returned within the daylight portion of the orbit and only when the interferometric mode is not operating, which leaves only 31.5 min for a 15-min swath.

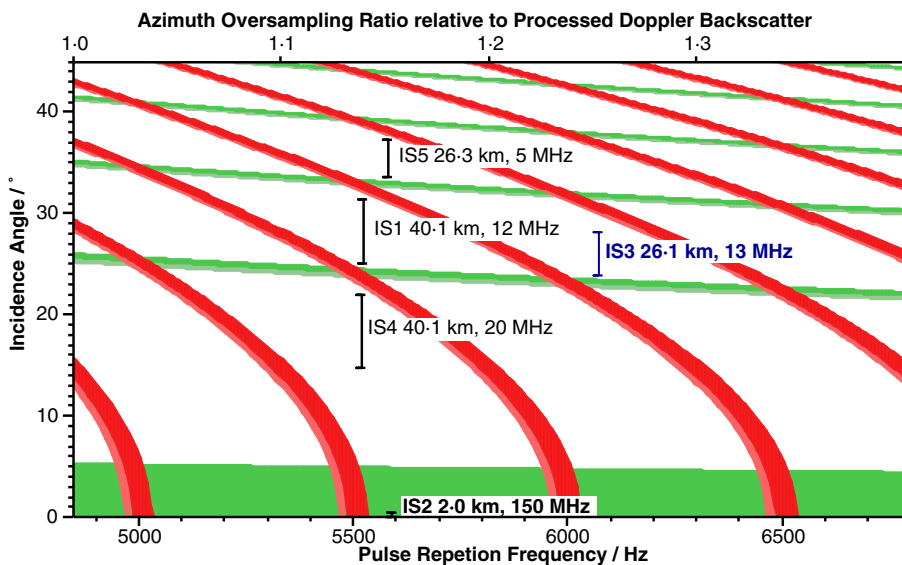


**Fig. 3** Swath selection diagram. Image swaths must avoid both the *red* (antenna transmitting) and *green* (nadir echos received) areas

Assuming the communications system can maintain an average downlink rate of  $1.0 \text{ MB s}^{-1}$ , these data volumes require 81.6 and 46.5 min to transmit to Earth, respectively. The operation of the interferometric mode is therefore limited by the available communications data rate and link time. At a downlink rate of  $1.0 \text{ MB s}^{-1}$ , EIAM-2 mode is limited to a maximum of 7 min and EIAM-1 to a maximum of 11 min of data collection; realistic limits at this downlink rate are 5 and 9 min respectively. Even with this mission scenario the downlink will take up to 28 min, placing high demands on existing ground stations. Figure 4 illustrates an example of the coverage that could be obtained

**Table 3** Interferometric operating modes of the EnVision antenna

	EIAM-1	EIAM-2
Fixed duty ratio	4%	
Pulse repetition frequency	6073 Hz	
Incidence angle	23.885–28.176°	
Ground range	125.999–152.099 km	
Look angle	22.692–26.736°	
Mode sensitivity	−19.49 dB	−16.49 dB
Range ambiguity	−38.62 dB	
Azimuth ambiguity	−27.20 dB	
Bandwidth	6.27 MHz	12.54 MHz
Sample rate	6.64 MHz	13.28 MHz
Full data rate	4.13 MB s <sup>−1</sup>	7.25 MB s <sup>−1</sup>
Reduced data rate	3.10 MB s <sup>−1</sup>	5.44 MB s <sup>−1</sup>
Range resolution	60.0 m	30.0 m

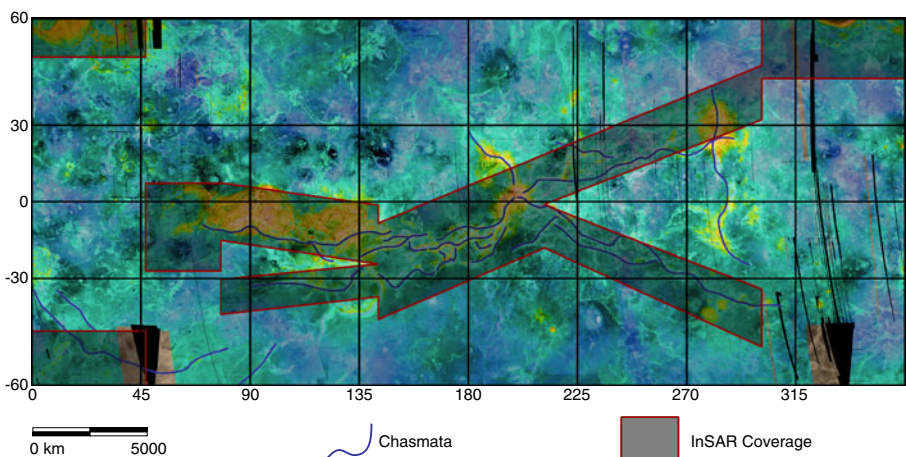


**Fig. 4** Example swath coverage in each mapping cycle. Possible InSAR coverage of the Venus surface, assuming EAIM-1, a radar imaging duration of 9 min and a complete cycle of 3763 orbits. Each orbit strip is 26.1 km wide, narrower than the lines of longitude at this scale. The map shows the effect of selective targeting of geologically interesting features, with some coverage extending beyond latitudes 60° N and 60° S

with 9-min per orbit operating in EAIM-1 after a full mapping cycle (243 days, 3763 orbits). Nearly 20% of the surface is covered, which includes the majority of interesting targets. While this is considered sufficient for delivery of the primary science goals, there are some important exceptions, such as Phoebe Regio, which might therefore be covered during Cycles 3, 4 and 7, or in Cycles later than 8 during an extended mission. Nonetheless, an improved downlink rate, closer to the practical limit of  $\sim 15 \text{ MB s}^{-1}$ , would greatly alleviate the data demands from the mission.

### 2.1.2 Radiometer and altimeter mode

Magellan obtained global topographic data with a vertical resolution of 30 m and radiometry data (at the SAR look angle) with an uncertainty of 2 K, from which the surface emissivity was derived. Both were at a spatial resolution of 10 km. Reflectivity and regional slope data were also derived from the altimeter data but because of the difference in look angle the reflectivity and emissivity data could not be combined to improve the brightness temperature estimate or derive atmospheric transmissivity.

In altimetric mode (EARAM), EnVision will target 60 pulses per second at nadir to determine the vertical ground range, even during interferometric mode operations, with one nadir pulse interleaved between every  $\sim 100$  side-looking SAR pulses. The radiometer will record the nadir radio emissions between altimeter pulses. However, because the SAR will be transmitting during interferometric mode operations, radiometry data can only be collected

during altimeter-only operations. Altimeter coverage will therefore be global but radiometer data will initially be collected only from the 80% of the surface not imaged during InSAR operations. Global coverage will be completed during Cycles 3 and 4 when InSAR operations target a different 20% of the surface.

During operation of the interferometric mode, the antenna beam can be electronically steered by up to  $\pm 25^\circ$  away from the boresight. This enables the antenna to direct approximately one in every 100 pulses at nadir to support altimetric data acquisition, with the remaining pulses targeted at  $24\text{--}28^\circ$  for the SAR data. The impact of 1 in 100 gaps in the SAR data stream has been shown to have minimal impact on InSAR data quality. The altimetric data must be streamed separately from the SAR data and processed independently, for which sufficient resources are provided within the RCE subsystem.

The same nadir-pointed data stream is used to acquire and process radiometric data. The full data rate received in the altimetric mode is  $67.0 \text{ kB s}^{-1}$  (with a 60 Hz sample rate) and the same is received during the integrated radiometer observations. However, the phase data is not needed in either case and 3-bit I, 3-bit Q adaptive quantisation is likely to be sufficient, so the data rate for transmission to Earth is reduced to only  $50.3 \text{ kB s}^{-1}$ . When operating independently of the interferometric mode, the antenna power demanded to run the altimetric and radiometric modes is only 1% of the interferometric mode. This mitigates the principal thermal constraint and enables operation of these modes for the whole of the daylight part of the orbit, giving a pole-to-pole swath and generating 137.0 MB of data per orbit.

At 60 Hz, the altimetric mode provides a data point every 115 m along track. To reduce the volume of data transmitted to Earth, a rolling average of 32 data points will be processed on board to determine the surface elevation to a vertical accuracy of about 1 m at a spatial resolution of 3600 m along track and 600 m across track. Each topographic track is separated by the orbital ground track spacing of 10.1 km, providing a final dataset with a spatial density of  $3.6 \times 10.1 \text{ km}^2$ .

By analysing the altimetric returns in the same way as was done for Magellan [17], reflectivity and regional slope data can also be derived. However, because the radiometer will look at the nadir radio emissions and averaged over the same interval as the altimeter, the two datasets can be directly correlated to determine C-band atmospheric transmissivity. Cross-correlating the data in this way improves the confidence in the detection of real emission sources, such as the still-warm lava flows recently inferred [8] from Magellan data.

Because the angular beamwidth of the SAR mode ( $\sim 4^\circ$ ) permits stereoscopic reduction between orbit pairs, a second source of topographic data, with a spatial resolution of about 120 m and a vertical resolution of better than 10 m, can be obtained from the part of planet imaged in the interferometric mode. Together, these topographic datasets provide an orders-of-magnitude improvement on even stereo SAR Magellan data, which has a spatial resolution of about 500 m.

## 2.2 Venus advanced accelerometer

To achieve interferometric SAR, EnVision's orbit must be known with an accuracy at least ten times better than Magellan. The Venus Advanced Accelerometer (VAA) consists of a 3-axis electrostatic accelerometer which in combination with Ka-band Doppler tracking (which suffers fewer distortion effects than Magellan's X-band tracking) and a more precise star tracker system (for spacecraft positioning) will improve the determination of EnVision's orbit by at least a factor ten compared to Magellan. VAA is based upon the  $\mu$ STAR accelerometer, which is a small, low mass and low power device (3 kg and 3 W, including the bias compensation mechanism and the interfaces). Its core is an accelerometer benefiting from the ONERA design heritage [13] that was successfully used in many recent space experiments, e.g., CHAMP, GRACE and GOCE.

The VAA science goal is to improve the resolution of the free-air gravity field to better than  $50 \text{ }\mu\text{m s}^{-2}$  and the geoid to 0.5 m in amplitude, both at a spatial resolution of 53 km (360th degree field determination), with global consistency. This apparently modest improvement will provide a quantum leap in understanding the deeper processes that generate discrete geological features such as coronae and volcanoes (which are generally not resolved in Magellan gravity data).

## 2.3 Venus emissivity mapper

The Venus Express mission has demonstrated the feasibility of mapping thermal emission from the surface using near-infrared spectral window regions lying between 0.8 and 1.8  $\mu\text{m}$ . Such mapping can reveal anomalies in surface temperature, e.g., from hot lava flows [25], and also anomalies in surface emissivity [39].

The Venus Emissivity Mapper (VEM) builds on experience from the analysis of data from Galileo/NIMS, Cassini/VIMS, and especially Venus Express/VIRTIS, to observe surface thermal emissions. Unlike those general-purpose imaging spectrometers, VEM is focused on observing the surface, mapping the ground in all of the near-infrared (NIR) atmospheric windows. In addition, several other bands are used to observe the clouds and water vapour in the 0 to 15 km altitude range that chemically and physically interacts with the surface. Figure 5 shows the placement and width of the VEM channels and the science themes addressed by each channel. Most channels contribute to more than one science theme, making VEM a very versatile instrument.

VEM builds on the heritage and lessons learned from VIRTIS on Venus Express, disentangling the surface and atmospheric contributions to the observed radiance using an improved version of algorithms developed to process VIRTIS surface data. It is designed to image Venus with an SNR at 1.31  $\mu\text{m}$  that is twice that of a 3-s exposure VIRTIS image. The sensitivities of the band centres and widths of VEM's filters will be  $\sim 5$  times less than

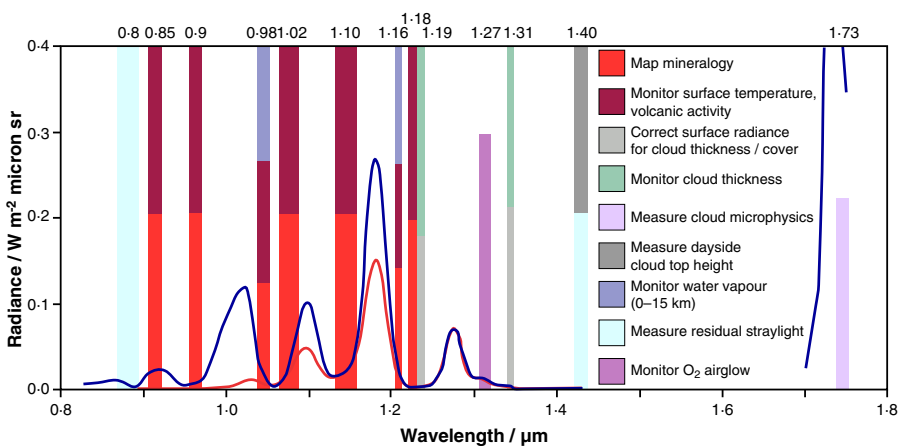


**Fig. 5** Spectral bands of the Venus emissivity mapper

VIRTIS, allowing more stable and accurate spectral mapping. Finally, VEM will have a baffle and will observe much of Venus in eclipse (possible from low orbit), dramatically decreasing the level of scattered light that affects VIRTIS.

While VEM is a new instrument, it uses well-established concepts for multi-spectral, push-broom imaging. The full instrument is a monoblock configuration with an internal optical bench. The VEM baseplate (the mechanical and thermal interface to the spacecraft), the electronic housing and the optical bench are machined as a single element from an aluminium billet. The detector and optics are mounted on the optical bench to ensure mechanical and thermal stability of the optical path. The box baffle is thermally linked directly to the baseplate, eliminating the baffle thermal load transfer to the optical elements. VEM's fully redundant electronic boards are located in a box under the optical bench and the instrument cover is wrapped in MLI.

VEM's telecentric optics provide consistent spectral bandpasses across the unobstructed  $66^\circ$  field of view. The resulting broad swath provides a wide surface coverage in each orbit. A filter array is mounted directly on the entrance window of the space-qualified HgCdTe detector. Filters are installed with surface-observing channels near the centre to minimise emission angle and the influence of the atmosphere. The two main cloud-observing filters are at the edges, to allow tracking of cloud movement for cloud correction of the surface band data. The filter array is mounted on the detector dewar with good thermal coupling to avoid wavelength drift of the filters due to thermal stress. VEM observes continuously in all spectral bands on the nightside and in one band over the dayside, where the  $0.9\text{-}\mu\text{m}$  band is used to monitor cloud movement. Spatial and spectral binning can be varied by software to adjust the data volume or the SNR.

## 2.4 EnVision doppler LIDAR

The relatively high power and high data rate requirements and low circular orbit of EnVision permit the deployment of a LIDAR instrument. However, a compact (<50 kg) Doppler LIDAR is a new development for Europe and consequently this is the lowest TRL instrument on EnVision. The instrument will provide direct measurement of mesospheric winds and study of cloud-top properties. Mesospheric winds on Venus have been inferred on the basis of temperature fields by assuming cyclostrophic balance [42] but this technique is indirect, is invalid at low and high latitudes, and is only strictly applicable to zonally-averaged wind fields. Direct measurement of mesospheric winds from a Doppler LIDAR will finally permit the measurement of mean circulation and of wind transients associated with dynamics at all latitudes, including the complex polar vortex region.

The second main function of the LIDAR is to return vertical profiles of the backscatter coefficient at the cloud-tops. These data will permit the study of the many morphological phenomena revealed by the Venus Monitoring Camera (VMC) on Venus Express that are apparently associated with waves and convection [37]. As yet it is unclear whether these features are caused by height differences in the cloud tops, by compositional differences, or by cloud microphysical variations. An important component of this will be the collection of data from the spiral arms and whorl-like structures associated with the polar vortices found in both the northern and southern hemispheres. The whorls are similar to structures seen in the core region of tropical cyclones and are smaller-scale circulations within the complex vertical structure of the polar vortex. LIDAR measurements of the cloud structure of hurricane Melissa [30] provided 15-m vertical profiling of its clouds and aerosols. Similar results are anticipated from EnVision, providing unprecedented detail of the internal structure of cyclonic systems on another planet. The LIDAR would also be able to study day-night and latitudinal differences in cloud-top structure. Dual-wavelength capability, e.g. 532 and 1064 nm, would enable discrimination between sub-micron ‘Mode 1’ haze particles known to exist in polar regions, and the larger ‘Mode 2’ main cloud deck particles.

## 2.5 Thermal infrared mesospheric mapping spectrometer

The measurements obtained by the LIDAR will be contextualised by a remote sounding suite. The Thermal Infrared Mesospheric Mapping Spectrometer (TIMMS), operating in the 5 to 25  $\mu\text{m}$  wavelength range, will measure temperature profiles from 65 to 90 km altitude on the dayside, providing context for the LIDAR’s direct wind measurements. It will also measure abundances of stratospheric constituents including CO, H<sub>2</sub>O and SO<sub>2</sub> and cloud-top temperatures. This will recover much of the science lost with the failure of the Planetary Fourier Spectrometer (PFS) instrument on Venus Express. PFS included 2 channels, the short wave channel from 1 to 5  $\mu\text{m}$  and the long wave channel from 5 to 45  $\mu\text{m}$  (Formisano et al. 2006); Venus

Express' VIRTIS imaging spectrometer has addressed the science goals of the short wave channel, leaving the goals of the long wave channel still to be addressed. The instrument proposed is under development for Marco Polo; it is compact (<3 kg), robust (no moving parts other than a scan/calibration mirror) and has a spectral resolution of  $5 \text{ cm}^{-1}$ . It is an imaging Fourier transform mapping spectrometer utilising a beam-shearing interferometer to generate a set of spatially resolved interferograms that are imaged onto an uncooled bolometer array, allowing spectral image cubes of the target body to be measured.

## 2.6 Spectrophotopolarimeter for planetary exploration

Completing the atmospheric science suite is the Spectrophotopolarimeter for Planetary EXploration (SPEX). The LIDAR's measurement of cloud-top structure returns vertical profiles of the backscatter coefficient. To convert this into the more meaningful quantities such as cloud particle number density requires further information about the cloud particles. This can be obtained by measuring polarisation and intensity phase functions, as was first demonstrated for Venus upper cloud by [24] who used Earth-based polarimetry data of Venus to determine that the Venus cloud on average consisted of sulphuric acid cloud droplets with a very narrow size distribution with a mean radius of  $1.05 \mu\text{m}$ . SPEX will measure the polarisation state as well as the intensity of light in the 400 to 800 nm range in order to reveal the microphysical properties of the cloud, which will improve the interpretation of the LIDAR data.

SPEX (Fig. 6) is an innovative, compact instrument. The spectropolarimetry is achieved by encoding the degree of linear polarisation (DoLP) and angle of linear polarisation (AoLP) of the incident light in the measured flux spectra using the technique of spectral modulation. The spectral modulation principle allows the polarisation optics to be very small and robust. The spectrally modulated spectrum is measured using a spectrometer and detector yielding sufficient spectral resolution. SPEX has the capability to measure spectra under different viewing angles while flying over a ground pixel. This way SPEX samples the flux and polarisation scattering phase function over a large range of scattering angles, yielding a precise characterisation of the atmospheric aerosols. Limb viewers can be employed for the study of high clouds and vertical profile information on aerosols. The design is very stiff, yet light (0.9 kg) and compact through the use of a monoblock construction. Modern production techniques of spark eroding and diamond turning eliminate the need for active alignment of the optical elements, other than the focusing of the spectrometer detector.

## 2.7 UV spectrometer channel

Complementing TIMMS will be a UV Spectrometer Channel (UVSC), which addresses two main science goals. Firstly, it will monitor  $\text{SO}_2$  abundances at

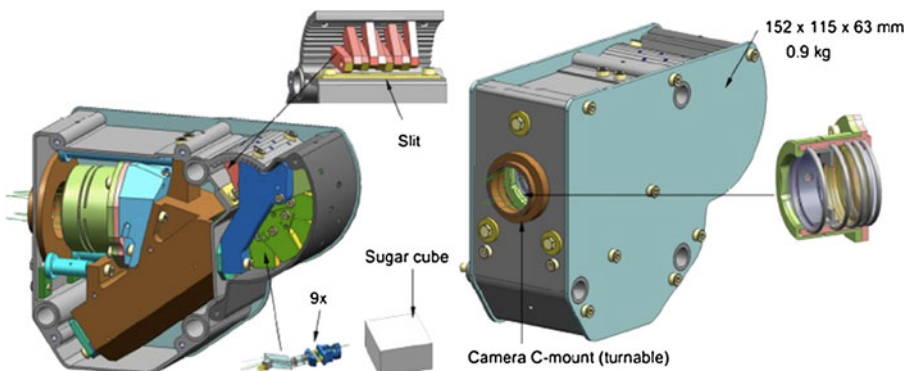


**Fig. 6** SPEX mechanical design. Mechanical design of SPEX showing the exterior, interior, and zooms of the imaging optics, beam combiner, and polarization pre-optics [45]

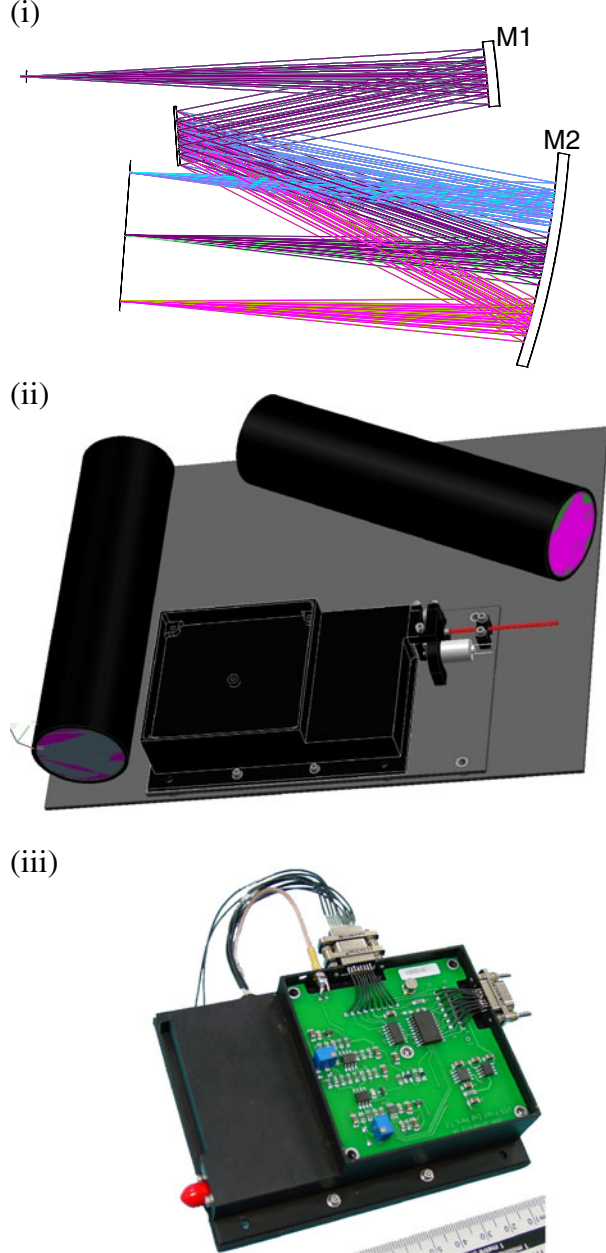
cloud-tops, which have been observed to vary by over an order of magnitude over timescales of 1 to 10 years [15, 35]. UVSC SO<sub>2</sub> data are thus vital for continuing the long-term time series analysis of SO<sub>2</sub> abundances, but for the first time these data will also be used in conjunction with surface science monitoring to determine whether SO<sub>2</sub> injections are correlated with volcanic activity.

Secondly, UVSC will monitor the spatial distribution of the still ‘unknown UV absorber’ that is responsible for more than half the solar energy absorption at Venus, with the advantage of synchronous LIDAR data to constrain the cloud-top structure. The proposed UVSC is a fibre-coupled grating spectrometer, with a spectral range of 180 to 360 nm and spectral resolution of 0.5 nm (Fig. 5). It is a clone of the instrument currently on the ExoMars TGO Orbiter payload as part of the NOMAD instrument, with the redundant (for Venus) visible capability removed, operating between 200 and 400 nm. The instrument has an extensive heritage of development for the ExoMars Rover and (now descoped) Lander, with additional telescopic entrance optics for application in orbit, and is extremely low mass (0.5 kg) and low power (2 W) by sharing the scan mirror and electronics with TIMMS (Fig. 7).

The UVSC optics consists of three distinct parts: a dual front-end telescopic viewing optics; a fibre optic selector mechanism; and an optical bench. These parts are direct copies of the instrument currently being built for the ExoMars Orbiter, prior to the descope of the entire landed static element. The spectrometer is based around a Czerny–Turner layout. The optical components are all housed within a light-tight enclosure and mounted on a carbon fibre baseplate.

It should be noted that this detailed spectroscopic study of the upper cloud layers may provide direct evidence for active volcanism. In July 2009, the Venus Monitoring Camera on Venus Express observed a region of unusually bright cloud, 30% brighter than previously observed [33].

**Fig. 7** UVSC optical bench layout. Simplified layout of the optical bench (*i*), a 3D-impression (*ii*) and photo of the optical bench (*iii*)



## 2.8 EnVision double-Langmuir probe

The resource requirements of the ELP, provided by the Swedish Institute of Space Physics (IRF), are modest, amounting to less than 1 kg mass and 2.3 W, including electronics. The instrument consists of two ~1 m sticks (not booms) and probes (Fig. 8) and has a very high TRL of 8. The instrument's

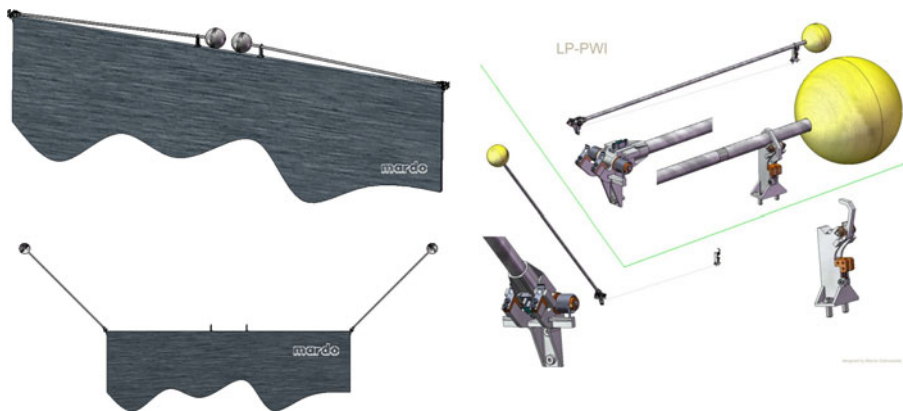


**Fig. 8** Double Langmuir probe schematics

science returns are greatly enhanced by operating in conjunction with the Venus Vector Magnetometer and both experiments will return significant science data during the aerobraking phase of the mission. The performance characteristics of the ELP are outlined in Table 4.

## 2.9 Venus vector magnetometer

VVM accomplishes high precision, ultra-high linearity and low noise measurements of magnetic field vector components, working in conjunction with the ELP to characterise the electric and magnetic fields induced at Venus. It is derived from the compact spherical coil (CSC) vector feedback magnetometer (VFM) of the Swarm mission, using the simple and reliable fluxgate principle. A dedicated development led to the vector fluxgate magnetometers for Ørsted, CHAMP and Ørsted-2/SAC-C drawing heavily from former mission heritage.

All three sensor components are placed in the common null field inside the homogeneous volume of the spherical coil. Each fluxgate element acts as a null field indicator and controls the feedback current of the corresponding outer coil. The coil current is an exact measure of the corresponding ambient magnetic field component. The CSC sensor is placed on the end of a boom with the interface electronics in the body of the spacecraft. VVM samples the

**Table 4** ELP performance characteristics

Electron number density ( $N_e$ )	$< 10^6 \text{ cm}^{-3}$ , 0 (DC) to 20 kHz
Ion density	$< 10^6 \text{ cm}^{-3}$ , <1 Hz
Electron temperature ( $T_e$ )	0.01 to a few eV, <1 Hz
Ion drift speed ( $V_{di}$ )	1 – 200 km s $^{-1}$ (depending on density), <1 Hz
Spacecraft potential	$\pm 20 \text{ V}$ , <1 Hz
Electric field (one component)	1 Hz to a few MHz

magnetic field at a rate of 50 vectors per second and has a full-scale range of  $\pm 65 \mu\text{T}$  and is accurate to 1 nT in each component over frequencies up to 4 Hz.

## 2.10 Venus interplanetary particle analyser

VIPA is based on the Galileo/Ulysses dust instrument and consists of a 0.1 mm thick gold foil of hemispherical shape with three grids at the entrance (entrance grid, charge grid, and shield), as well as an ion collector and channeltron detector. The maximum sensitive area (for particles moving parallel to the sensor axis) is  $0.1 \text{ m}^2$ . Upon impact the particle produces a plasma whose charge carriers are separated by an electric field between the target and the ion collector. The sensitivity of the instrument is dependent on the speed of the impacting particles, ranging from  $1.2 \times 10^{-13}$  at  $5 \text{ km s}^{-1}$  to  $2.0 \times 10^{-15}$  at  $20 \text{ km s}^{-1}$  [22].

The nature of hot neutral atom (HNA) escape from Venus would be useful to characterise. In its current design and location on the rear of the spacecraft (pointing away from Venus), VIPA is unable to measure these HNAs; future developments and a forward position may enable a modified VIPA to do so.

## 3 Mission profile

EnVision is planned to be fuelled to near the mass limit ( $\sim 1500 \text{ kg}$ ) for a Soyuz-Frigat launch from Kourou to interplanetary transfer orbit, primarily to deliver the spacecraft into a low circular orbit at Venus and to ensure precise orbit maintenance for the 5-year nominal mission. The radar antenna is designed to fit within the Soyuz fairing in its final fixed state, to avoid the complexity and additional mass of the folded Sentinel-1 antenna. Three launch opportunities have been identified, in March 2020, October 2021 and May 2022, with a transfer time of about 150 days in each case.

Following Venus capture, EnVision will undertake six to twelve months of aerobraking to circularise the orbit. The manoeuvre will involve using both the solar panels and the radar antenna as ‘sails’ to increase the drag experienced and so reduce the orbital eccentricity. The steerable high gain antenna will be stowed at the rear of the spacecraft body to avoid instabilities occurring during aerobraking.

The remaining fuel is required for orbital station keeping to ensure that EnVision returns to within 100 m of its starting position at the end of each 243-day orbit cycle. This strict requirement is to allow the repeated collection of InSAR data each cycle by providing a baseline suitable for interferometry. The data-intensive radar system has its own dedicated data handling system processing the  $16 \text{ MB s}^{-1}$  or more data rates that the system can acquire. In total, EnVision’s payload generates 1840 MB of data per 93-min orbit. In the worst case scenario (near superior conjunction), these data must be

returned from nearly 1.7 AU in the ~30 min of daylight remaining after InSAR operations.

EnVision therefore takes advantage of development work for Bepi Columbo, using its 1.5-m diameter X/Ka dual-band steerable high temperature high gain antenna (HTHGA) but provides a transmission power level of 260 W to allow minimum data rates of at least  $1.5 \text{ MB s}^{-1}$  at 1.7 AU and up to  $15 \text{ MB s}^{-1}$  closer to Earth.

The nominal 5-year mission provides 8 cycles of 3763 polar orbits, with each cycle equal to one sidereal Venus day (243 Earth days), enabling EnVision to acquire data at all points on the surface and returning to the same orbital position, for interferometric purposes, at the end of each cycle.

## 4 Future development

The concept of an InSAR mission was first proposed before Venus Express but had to wait until the Sentinel-1 programme for the technology to develop to the point at which it is now feasible to not only undertake such an ambitious mission but also to be able to return and process the wealth of data it will provide. Had it been selected, EnVision would have been the first radar mission to Venus since NASA's Magellan more than 30 years earlier.

EnVision is an ambitious proposal and one that is technically demanding, particularly given the breadth of its instrument suites, but it is the Venus environment itself that is perhaps the most challenging. Research is underway to develop an active cooling system to allow the radar to image the whole planet during each orbit cycle in both H and V polarisations, permitting a ten-fold increase in the science data returned. Sentinel-1 is a 7-year nominal mission but has consumables for 12 years; it is very likely that EnVision could similarly continuously operate for 10 years, in a 5-year nominal and 5-year extended mission profile. Such a programme could provide 80% InSAR coverage of the planet at existing data rates, or detect changes in rates of vertical ground deformation arising from, for example, magma chamber inflation and deflation, as well as providing a longer baseline for the detection of discrete seismic, mass wasting or volcanic events.

Similarly, a dual-wavelength Doppler LIDAR capable of continuous operation is planned that would provide both day and night side stratospheric wind profiles and upper cloud deck properties. An energetic ion/neutral/electron spectrometer, developed from ASPERA-4 on Venus Express, will provide a valuable addition to the Ionospheric Science Suite, complementing both the dust collector and Langmuir probe data and refining estimates of atmospheric inputs and escape.

The data volumes generated by these improved experiments are considerably higher than even the nominal proposal. However, ESA is under multifaceted pressure to increase its data-handling and ground resource capabilities, permitting greater science data returns from all its future deep space

missions; such changes would allow the more ambitious data returns outlined above.

EnVision is a concept that was inconceivable a decade ago when Venus Express was proposed. Despite its surprisingly low cost and mass, its future development promises even greater science returns. When the future EnVision flies, it will be the first to record the geological heartbeats of another world. An ambassador for European cooperation, expertise and technological capability, it will provide scientists with an invaluable insight into the workings of the only other Earth-like planet in the Solar System.

**Acknowledgement** The authors would like to thank ESA for their thorough evaluation of this proposed mission and the valuable feedback provided.

Dr Mitchell's work was carried out at the Jet Propulsion Laboratory, California Institute of Technology, under a contract with the National Aeronautics and Space Administration.

## References

1. Anderson, F.S., Smrekar, S.E.: Global mapping of crustal and lithospheric thickness on Venus. *J. Geophys. Res.* **111**, E08006 (2006)
2. Baker, V.R., Komatsu, G., Parker, T.J., Gulick, V.C., Kargel, J.S., Lewis, J.S.: Channels and valleys on Venus: Preliminary analysis of Magellan data. *J. Geophys. Res.* **97**, 13421–13444 (1992)
3. Barabash, S., Fedorov, A., Sauvaud, J.A., Lundin, R., Russell, C.T., Futaana, Y., Zhang, T.L., Andreasson, H., Brinkfeldt, K., Grigoriev, A., Holmstrom, M., Yamauchi, M., Asamura, K., Baumjohann, W., Lammer, H., Coates, A.J., Kataria, D.O., Linder, D.R., Curtis, C.C., Hsieh, K.C., Sandel, B.R., Grande, M., Gunell, H., Koskinen, H.E.J., Kallio, E., Riihela, P., Sales, T., Schmidt, W., Kozyra, J., Krupp, N., Franz, M., Woch, J., Luhmann, J., McKenna-Lawlor, S., Mazelle, C., Thocaven, J.-J., Orsini, S., Cerulli-Irelli, R., Mura, M., Milillo, M., Maggi, M., Roelof, E., Brandt, P., Szego, K., Winningham, J.D., Frahm, R.A., Scherrer, J., Sharber, J.R., Wurz, P., Bochsler, P.: The loss of ions from Venus through the plasma wake. *Nature* **450**, 650–653 (2007)
4. Brace, L.H., Kasprzak, W.T., Taylor, H.A., Theis, R.F., Russell, C.T., Barnes, A., Mihalov, J.D., Hunten, D.M.: The iontail of Venus: Its configuration and evidence for ion escape. *J. Geophys. Res.* **92**, 15–26 (1987)
5. Basilevsky, A.T., Head, J.W.: The geologic history of Venus: A stratigraphic view. *J. Geophys. Res.* **103**, 8531 (1998)
6. Basilevsky, A.T., Head, J.W.: Rifts and large volcanoes of Venus: global assessment of their age relations with regional plains. *J. Geophys. Res.* **105**, 24583 (2000)
7. Biggs, J., Bergman, E., Emmerson, B., Funning, G., Jackson, J., Parsons, B., Wright, T.: Fault identification for buried strike-slip earthquakes using InSAR: the 1994 and 2004 Al Hoceima, Morocco earthquakes. *Geophys. J. Int.* **166**, 1347–1362 (2006)
8. Bondarenko, N.V., Head, J.W., Ivanov, M.A.: Present-day volcanism on Venus: evidence from microwave radiometry. *Geophys. Res. Lett.* **37**, 23202 (2010)
9. Bullock, M.A., Grinspoon, D.H.: The stability of climate on Venus. *J. Geophys. Res.* **101**, 7521 (1996)
10. Campbell, B.A.: Surface formation rates and impact crater densities on Venus. *J. Geophys. Res.* **104**, 21951 (1999)
11. Carter, L.M., Campbell, D.B., Campbell, B.A.: Impact crater related surficial deposits on Venus: Multipolarization radar observations with Arecibo. *J. Geophys. Res.* **109**, 06009 (2004)
12. Chang, Wu-L., Smith, R.B., Wicks, C., Farrell, J.M., Puskas, C.M.: Accelerated uplift and magmatic intrusion of the Yellowstone caldera, 2004 to 2006. *Science* **318**, 952–956 (2007)

13. Christophe, B., Foulon, B., Levy, A., Anderson, J.D., Sumner, T.J., Bertolami, O., Gil, P., Páramos, J., Progrebenko, S.V., Gurtvis, L., Reynaud, S., Courty, J.-M., Asmar, S.W., Métris, G., Bério, P., Bingham, R., Kent, B., Olsen, O., Andersen, P.H., Dittus, H., Lämmerzahl, K., Theil, S., Rievers, B., Bremer, S.: Gravity advanced package, an accelerometer package for Laplace or tandem missions. In: Charbonnel, C., Combes, F., Samadi, R. (eds.) Proceedings of the Annual meeting of the French Society of Astronomy and Astrophysics. SF2A, pp. 103–106. (2008)
14. Ebmeier, S.K., Biggs, J., Mather, T.A., Wadge, G.: Steady downslope movement on the western flank of Arenal Volcano, Costa Rica. *Geochem. Geophys. Geosystems.* **11**, 12004 (2010). doi:[10.1029/2010GC003263](https://doi.org/10.1029/2010GC003263)
15. Esposito, L.W.: Long term changes in Venus sulfur dioxide. *Adv. Space Res.* **5**, 85–90 (1985)
16. Florensky, C.P., Basilevsky, A.T., Kryuchkov, V.P., Kusmin, R.O., Nikolaeva, O.V., Pronin, A.A., Chernaya, I.M., Tyuflin, Y.S., Selivanov, A.S., Naraeva, M.K., Ronca, L.B.: Venera 13 and Venera 14: sedimentary rocks on Venus? *Science* **221**, 57–59 (1983). doi:[10.1126/science.221.4605.57](https://doi.org/10.1126/science.221.4605.57)
17. Ford, P.G., Pettengill, G.H.: Venus topography and kilometer-scale slopes. *J. Geophys. Res.* **97**, 13103–13114 (1992)
18. Fournier, T.J., Pritchard, M.E., Riddick, S.N.: Duration, magnitude, and frequency of subaerial volcano deformation events: new results from Latin America using InSAR and a global synthesis. *Geochem. Geophys. Geosystems.* **11**, Q01003, 29 (2010). doi:[10.1029/2009GC002558](https://doi.org/10.1029/2009GC002558)
19. Fox, J.L.: Morphology of the dayside ionosphere of Venus: implications for ion outflows. *J. Geophys. Res.* **113**, E11001 (2008). doi:[10.1029/2008JE003182](https://doi.org/10.1029/2008JE003182)
20. Ghail, R.C.: Structure and evolution of southeast Thetis Regio. *J. Geophys. Res.* **107**, 5060 (2002)
21. Gilmore, M.S., Collins, G.C., Ivanov, M.A., Marinangeli, L., Head, J.W.: Style and sequence of extensional structures in tessera terrain, Venus. *J. Geophys. Res.* **103**, 16813 (1998)
22. Grün, E., Zook, H.A., Baguhl, M., Balogh, A., Bame, S.J., Fechtig, H., Forsyth, R., Hanner, M.S., Horanyi, M., Kissel, J., Lindblad, B.A., Linkert, D., Linkert, G., Mann, I., McDonnell, J.A.M., Morfill, G.E., Phillips, J.L., Polanskey, C., Schwehm, G., Siddique, N., Staubach, P., Svestka, J., Taylor, A.: Discovery of Jovian dust streams and interstellar grains by the Ulysses spacecraft. *Nature* **362**, 428–430 (1993)
23. Guest, J.E., Stofan, E.R.: A new view of the stratigraphic history of Venus. *Icarus* **139**, 55 (1999)
24. Hansen, J.E., Hovenier, J.W.: Interpretation of the polarization of Venus. *J. Atmos. Sci.* **31**, 1137–1160 (1974)
25. Hashimoto, G.L., Imamura, T.: Elucidating the rate of volcanism on Venus: detection of lava eruptions using near-infrared observations. *Icarus* **154**, 239 (2001)
26. Johnson, C.L., Richards, M.A.: A conceptual model for the relationship between coronae and large-scale mantle dynamics on Venus. *J. Geophys. Res.* **108**, 5058 (2003)
27. Jones, A.P., Pickering, K.: Evidence for aqueous ?uid – sediment transport and erosional processes on Venus. *J. Geol. Soc. London* **160**, 319–327 (2003)
28. Komatsu, G., Baker, V.R.: Meander properties of Venusian channels. *Geology* **22**, 67 (1994)
29. Komatsu, G., Gulick, V.C., Baker, V.R.: Valley networks on Venus. *Geomorph.* **37**(3–4), 225–240 (2001)
30. Kovacs, T.A., McCormick, M.P.: Observations of typhoon Melissa during the Lidar In-space Technology Experiment (LITE). *J. Appl. Med.* **42**, 1003–1013 (2003)
31. Kumar, P.: An alternative kinematic interpretation of Thetis boundary shear zone, Venus: evidence for strike-slip ductile duplexes. *J. Geophys. Res.* **110**, 07001 (2005)
32. Lammer, H., Lichtenegger, H.I.M., Biernat, H.K., Erkaev, N.V., Arshukova, I.L., Kolb, C., Gunell, H., Lukyanov, A., Holmstrom, M., Barabash, S., Zhang T.L., Baumjohann W.: Loss of hydrogen and oxygen from the upper atmosphere of Venus. *Planet. Space Sci.* **54**(13–14), 1445–1456 (2006)
33. Limaye, S.S., Markiewicz, W.J., Titov, D.V.: A bright spot on Venus. *EGU abstracts, 2010EGUGA.1211468L* (2010)
34. Luhmann, J.G., Kasprzak, W.T., Russell, C.T.: Space weather at Venus and its potential consequences for atmospheric evolution. *J. Geophys. Res.* **112**, E04S10 (2007). doi:[10.1029/2006JE002820](https://doi.org/10.1029/2006JE002820)

35. Marcq, E., Belyaev, D., Montmessin, F., Fedorova, A., Bertaux, J.-L., Vandaele, A.C., Neefs, E.: An investigation of the SO<sub>2</sub> content of the Venusian mesosphere using SPICAV-UV in nadir mode. *Icarus* **211**, 58–69 (2011)
36. Marinangeli, L., Gilmore, M.S.: Geologic evolution of the Akna Montes-Atropos Tessera region, Venus. *J. Geophys. Res.* **105**, 12053 (2000)
37. Markiewicz, W., Titov, D., Limaye, S., Keller, H., Ignatiev, N., Jaumann, R., Thomas, N., Michalik, H., Moissl, R., Russo, P.: Morphology and dynamics of the upper cloud layer of Venus. *Nature* **450**, 633 (2007)
38. McComas, D.J., Spence, H.E., Russell, C.T., Saunders, M.A.: The average magnetic field draping and consistent plasma properties of the Venus magnetotail. *J. Geophys. Res.* **91**, 7939–7953 (1986)
39. Müller, N., Helbert, J., Hashimoto, G., Tsang, C., Erard, S., Piccioni, G., Drossart, P.: Venus surface thermal emission at 1 μm in VIRTIS imaging observations: evidence for variation of crust and mantle differentiation conditions. *J. Geophys. Res.* **113**, 1–21 (2008)
40. Nimmo, F., McKenzie, D.: Volcanism and tectonics on Venus. *Ann. Rev. Earth Planet. Sci.* **26**, 23–51 (1998)
41. Phillips, J.L., Luhmann, J.G., Russell, C.T.: Dependence of Venus ionopause altitude and ionospheric magnetic field on solar wind dynamic pressure. *Adv. Space Res.* **5**, 173–176 (1985)
42. Piccialli, A., Titov, D.V., Grassi, D., Khatuntsev, I., Drossart, P., Piccioni, G., Migliorini, A.: Cyclostrophic winds from the visible and infrared thermal imaging spectrometer temperature sounding: a preliminary analysis. *J. Geophys. Res.* **113**, E00B11 (2008)
43. Schubert, G., Sandwell, D.T.: A global survey of possible subduction sites on Venus. *Icarus* **117**, 173–196 (1995)
44. Smrekar, S.E., Stofan, E.R., Mueller, N., Treiman, A., Elkins-Tanton, L., Helbert, J., Piccioni, G., Drossart, P.: Recent hotspot volcanism on venus from VIRTIS emissivity data. *Science* **328**, 605 (2010)
45. Snik, F., Rietjens, J.H.H., van Harten, G., Stam, D.M., Keller, C.U., Smit, J.M., Laan, E.C., Verlaan, A.D., der Horst, R., Navarro, R., Wielinga, K., Moon, S.G., Voors, R.: SPEX: the spectropolarimeter for planetary exploration. In: Proc. SPIE 7731, 77311B (2010). doi:[10.1117/12.857941](https://doi.org/10.1117/12.857941)
46. Stevens, N.F., Wadge, G., Williams, C.A.: Post-emplacement lava subsidence and the accuracy of ERS InSAR digital elevation models of volcanoes. *Int. J. Remote Sens.* **22**, 819–828 (2001)
47. Stofan, E.R., Brian, A.W., Guest, J.E.: Resurfacing styles and rates on Venus: assessment of 18 Venusian quadrangles. *Icarus* **173**, 312–321 (2005)
48. Taylor, F., Grinspoon, D.: Climate evolution of Venus. *J. Geophys. Res.* **114**, E00B40 (2009)
49. Tuckwell, G., Ghail, R.C.: A 400-km-scale strike-slip zone near the boundary of Thetis Regio, Venus. *Earth Planet. Sci. Lett.* **211**, 45–55 (2003)
50. Turcotte, D.: An episodic hypothesis for Venusian tectonics. *J. Geophys. Res.* **98**, 17061–17068 (1993)
51. Turcotte, D.: How does Venus lose heat? *J. Geophys. Res.* **100**, 16931 (1995)
52. Turcotte, D., Morein, G., Roberts, D., Malamud, B.D.: Catastrophic resurfacing and episodic subduction on Venus. *Icarus* **139**, 49–54 (1999)
53. Waltham, D., Pickering, K., Bray, V.: Particulate gravity currents on Venus. *J. Geophys. Res.* **113**, 02012 (2008)
54. Wicks Jr, C., Thatcher, W., Dzurisin, D.: Migration of fluids beneath Yellowstone caldera inferred from satellite radar interferometry. *Science* **282**, 458 (1998)
55. Zebker, H.A., Rosen, P.A., Goldstein, R.M., Gabriel, A., Werner, C.L.: On the derivation of coseismic displacement fields using differential radar interferometry: the Landers earthquake. *J. Geophys. Res.* **99**, 19617 (1994)